Noise effects on the Berry phase

Andrea Agazzi
Simon Berger
Laboratory for Solid State Physics
ETH Zürich, Switzerland

04.03.2012

Abstract

The aim of this brief project is to explore the theoretically claimed resilience of quantum gates based on the Berry phase to open system effects such as noise. This has been done by simulating the gate in the presence of gaussian white noise first, and implementing it in an experiment subsequently. Particular attention has been paid to the numerical creation of noise. As an ultimate step, the results of both simulation and experimental measurement have been compared to the theory. We noticed a very good agreement in the average phase both in the presence and in the absence of noise for both simulation and experiment. A more limited agreement with theoretical predictions is displayed by other quantities (e.g. visibility).

Contents

1 Introduction

In recent years, physicists have been trying to develop methods to implement a completely new concept of computation based on quantum effects such as entanglement or spin. This would allow, besides the application of quantum algorithms such as the Grover search algorithm, which are expected to solve so-called NP problems in polynomial time, a deeper understanding of the fundamental laws of quantum mechanics and the possibility of more faithful quantum mechanics simulations.

On the other hand, an hypothetical quantum computer should satisfy some requirements, as mentioned in the famous $5 + 2$ DiVincenzo criteria [1]. Various possible architectures for quantum gates have been proposed (e.g. superconducting circuits [2], ion traps [3], semiconductor quantum dots [4], NMR [1]). Each of them displays different features, making them more or less promising with respect to the one or to the other of these requirements.

In particular, each of these architectures has to guarantee a long coherence time of the quantum system in order to be able to perform operations, and still read out the result of the computation. One of the most important elements triggering the decoherence of the qubit is of course its interaction with the environment inducing noise.

It is usually very difficult to avoid such fluctuations, in particular in the case of a possibly wide application of these quantum devices and to use them in non ideal situations, i.e. different from those of experimental laboratories. It is therefore desirable for a quantum device to be resilient to open system effects.

A quantum gate claiming to display this feature is the quantum gate based on Berry phase [5]. The fundamental idea of this gate is to use the geometric rather than the dynamic phase of the qubits' quantum state to perform computations. In fact the Berry phase is only dependent on the path followed by the Hamiltonian of the system and not on the time needed to complete it, and is therefore claimed to be only slightly affected by noise.

Our purposes in this brief project are to explore both theoretically (by means of theoretical investigations and simulations) and experimentally (by physically applying noise) the response of the gate to different kinds of noise.

2 Theory

In this section we explore in a purely theoretical way how the Berry phase of a spin-1/2 particle is affected by fluctuations in the control parameters, with the control parameters varying cyclically in the parameter space.

2.1 Fundamental concept

As mentioned in the introduction, the geometric phase gates are believed to be a very interesting candidate for noise-resilient quantum gates. In short, for the example of a spin-1/2 particle in a magnetic field B varying cyclically and adiabatically, this is due to the fact that the geometric phase has a geometric nature, i.e. its magnitude is not determined by the dynamics of the system (neither by energy nor by evolution time) but purely by the solid angle subtended to the evolution path in the parameter space. In particular, in the case of the magnetic field B precessing around the z-axis with precession angle ϑ, for a full precession cycle the geometric phase gained by the quantum state $|0\rangle$ is given by:

$$\phi_g^0 = -\pi(1 - \cos\vartheta) \tag{1}$$

The dynamic phase can be easily calculated by integrating the Larmor frequency over time. This has however not been done because it can cleverly be cancelled out with experimental methods explained in Section 4.

2.2 Berry phase in a classical fluctuating field

After a generic investigation of the phenomenon we will now study in detail how some experimentally relevant parameter of a spin-1/2 particle are affected by the presence of a classical fluctuating field. In particular, we will explore the parameters of Berry phase and visibility, where the latter is defined as the length of the Bloch vector describing the system. The formulas describing the evolution of such parameters formulas will the be extremely useful for e.g. measurement predictions and comparison with actual measurement results.

2.2.1 Assumptions

In this theoretical analysis, we are making the following assumptions on the experimental situation. All these assumptions except the third one coincide with those made in Ref. [6].

1. **Adiabaticity of the drive**: the magnetic field B is varied adiabatically, i.e. slowly with respect to the Larmor frequency, so that the instantaneous energy eigenstates follow the direction of B.

2. **Noise power**: the noise intensity is assumed to be much smaller than the control field B_0 itself. This allows us to linearize most of the equations concerning the noise field.

3. **Noise direction**: the fluctuations of the drive field are assumed to be only on the z direction. The x and y components of noise are not affected by noise. This is the only assumption which has not been made in Ref. [6].

4. **Adiabaticity of the fluctuating field**: we assume that the fluctuations are adiabatic.

5. **Noise spectrum**: the noise has been assumed to be part of an Ornstein-Uhlenbeck (OU) process. In particular, this means that it is a Gaussian process, it is Markovian with a Lorentzian spectrum. Further explanations for these assumptions are given below.

In particular, according to Ref. [6], by assuming that the noise is describe by an OU Process, is must display the following features:

- *Gaussian Power Spectrum*

  The total noise per bandwidth unit which adds to the drive must be Gaussian distributed with expectation value 0 and standard deviation σ_3.

- *Lorenzian Frequency Spectrum*

  In frequency space, the fourier spectrum of the noise must be Lorenzian distributed around the average frequency f_3 of the field with bandwidth Γ_3.
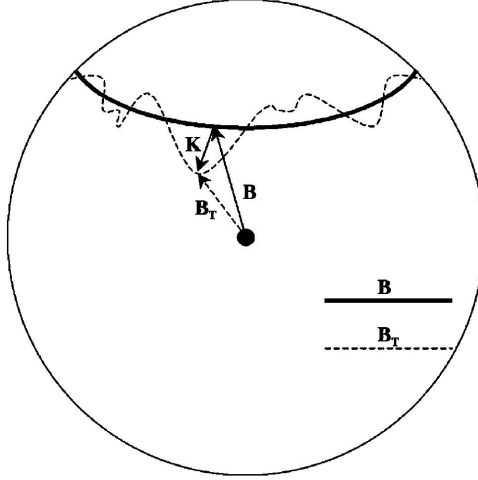
Figure 1: Sketch of the effect of noise on the state evolution in the Bloch sphere [6].

- *Markovian Process*

  A Markovian process is a memoryless process. This means that the noise at a given time is not influenced by the precedent one.

2.2.2 Theoretical expectations

Under the assumptions listed above, we can compute the effect of such a noise on the geometric phase and on the visibility of the system by following the steps described in Ref.[**?**]. First, we write the Hamiltonian of the system:

$$H(t) = \frac{1}{2}\mathbf{B}_T(t) \cdot \boldsymbol{\sigma} \tag{2}$$

where $\boldsymbol{\sigma} = (\sigma_x, \sigma_y, \sigma_z)$, σ_i are the Pauli operators, and $\mathbf{B}_T(t)$ is the total applied magnetic field, which can be expressed as a sum of the drive field in the absence of noise $\mathbf{B}_0$ and the noise field $\mathbf{K}$

$$\mathbf{B}_T = \mathbf{B}_0 + \mathbf{K} \tag{3}$$

with $\mathbf{K} = K\vec{e}_z$ because of the assumption made on the direction of the noise field. The Hamiltonian of the system can therefore be explicitly rewritten:

$$H(t) = \frac{1}{2}[\boldsymbol{\sigma} \cdot \mathbf{B}_0(t) + \sigma_z K(t)] \tag{4}$$

6

In the absence of noise ($\mathbf{K} = 0$), $\mathbf{B}_T = \mathbf{B}_0$ and the geometric phase acquired by the system over the course of a cycle is given by:

$$\gamma_B^0 = \oint \mathbf{A} d\boldsymbol{\lambda} = \pi \cos(\vartheta) \tag{5}$$

where $\mathbf{A} = \langle \uparrow_n | \boldsymbol{\nabla}_\lambda | \uparrow_n \rangle$ is called Berry connection, $| \uparrow_n \rangle$ are the eigenstates of the system depending on the direction of $\mathbf{B}$ and λ are the control parameters, in this case the direction of B, and therefore the angles (ϑ, φ). It can be proven that the ϑ component of $\mathbf{A}$ vanishes, we will therefore restrict our analysis to the A_φ component of the connection. In the case of non vanishing noise ($K \neq 0$) we get for the Berry phase

$$\gamma_B = \gamma_B^0 + \frac{\pi}{T} \int_0^T \left[\frac{K_z}{B_0} - \frac{B_{0z}}{B_0^3} \mathbf{B}_0 \cdot \mathbf{K} \right] dt \tag{6}$$

From this expression it can be shown that the probability distribution of γ_B is a Gaussian distribution as well, whose mean value is the noiseless Berry phase γ_B^0 and whose standard deviation is

$$\sigma_\gamma^2 = 2\sigma_z^2 \left(\frac{\pi \sin^2 \vartheta_0}{T B_0} \right)^2 \left[\frac{\Gamma T - 1 + e^{-\Gamma T}}{\Gamma^2} \right], \tag{7}$$

where $B_0 = |\mathbf{B_0}|$, ϑ_0 is the polar angle of the path without noise and T is the period of one cycle. Furthermore, the variance of the dynamical phase can be computed, and its effects on the coherence of the system (the length of the Bloch vector after having been averaged over the expected distribution of results) have to be taken into account with the ones coming from the variance of the geometric phase. It can be seen that the coherence of system after a time T is shrunk by a factor $\exp(-2\sigma_\alpha^2)$, where σ_α is given by:

$$\sigma_\alpha^2 = 2 \frac{\sigma_z^2}{B_0^2} \left(\frac{\pi \sin^2 \vartheta_0}{T} + B_0 \cos \vartheta_0 \right)^2 \left[\frac{\Gamma T - 1 + e^{-\Gamma T}}{\Gamma^2} \right] \tag{8}$$

In the RHS of equation (8), we recognize two terms, one being of geometrical nature ($\propto 1/T$) and the other of dynamical ($\propto B_0 \propto \omega_{Bohr}$). In the adiabatic regime we assumed before ($T \gg 1/B_0$), the first term is much smaller than the second. We can therefore conclude that the main contribution to dephasing has dynamical rather than geometrical origin.

3 Simulations

After having studied the effects of noise on the geometric phase of a spin-1/2 particle we are ready to simulate the effects of noise on the geometric phase acquired by the transmon, a solid state qubit embedded in a transmission line.

For our purposes, the behavior of the transmon/resonator system is very similar to the one of an atom interacting with an external EM field (for this reason it is also called artificial atom). This system is therefore not exactly equal to the one studied in section 2 because of the presence, in addition to the ground and excited state, of higher energy levels. However, if kept between the ground and first excited state, we expect its response to noise to be very close to the one predicted above for a spin-1/2 particle.

3.1 Simulation code

The program chosen to run the simulations is Mathematica and the source file has been written by slightly modifying an already existing simulation of the Berry phase of the transmon without noise.

With this simulation, we want to describe our experimental setup as closely as possible. In fact, the program describes a spin-echo experiment, where the qubit is manipulated as shown in Fig. 2: after the Hamiltonian of the system has run his cyclic path, a π-pulse is applied and the Hamiltonian runs the same path but this times backwards. In this way, the dynamical phase is cancelled out, whereas the geometric phase is doubled.

In principle, the simulation solves the Schrödingier Equation of the system in the rotating frame, where the Hamiltonian is given by:

$$H(t) = \frac{1}{2}\boldsymbol{\sigma} \cdot \mathbf{B}_T(t) = \frac{1}{2}[\boldsymbol{\sigma} \cdot \mathbf{B}_0(t) + \sigma_z K(t)] \tag{9}$$

where in the case of the transmon qubit we have:

$$\mathbf{B}_T(t) = \begin{pmatrix} \Omega_x \\ \Omega_y \\ \Delta \end{pmatrix} \tag{10}$$

with $\Delta = \omega_q - \omega_d$ the detuning between the frequency of the qubit ω_q and the frequency of the drive ω_d, $(\Omega_x, \Omega_y) = \Omega(\sin(\phi), \cos(\phi))$ are the I and Q quadratures of the drive, with Ω the drive amplitude and ϕ the drive phase.

It is easy to notice that the Hamiltonian of this system is analogous to the one describing a spin-1/2 particle in an external magnetic field as described in Eq. 2.

The simulation program allows us to control all relevant parameters: detuning, pulse duration, drive amplitude, direction of the path of the Hamiltonian (clockwise,anti-clockwise), adiabaticity, and the noise.

In order to simulate the response of our system to the application of noise we have to apply a fluctuating field to the z-component of $\mathbf{B}_T$. In our frame this is equivalent to keeping Ω fixed and shifting the detuning around an average value Δ_0. Because of the assumption of low frequency of the noise, we can approximate it to be constant over a pulse sequence. Our problem reduces therefore to applying a random normally distributed constant detuning to the average detuning Δ_0.
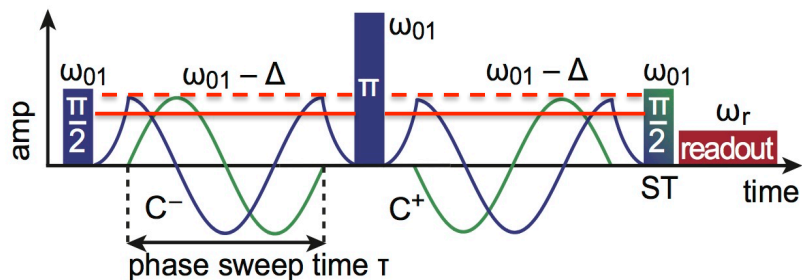

Figure 2: Sketch of the applied pulse sequence. In this figure it is displayed how noise is applied to the system: the detuning in the absence of noise Δ_0 (dashed red line) is shifted for every experiment by a random value so that the final detuning Δ is given by the red continuous line.

In fact, the implemented noise generation method can be summarized as follows: first, a sample of constant detuning pulses with detuning frequency Δ_0 was created. Then, a normal distributed random number with expectation value 0 and variance σ_3 (normal (o, σ_3) distribution) was generated for every element of the sample and a constant function with that value was added to the original detuning pulse.

The Berry phases acquired by the qubit for geometric spin-echo pulse sequences with fixed drive amplitude and the detuning pulses of the sample were then computed and collected in an histogram. This has been done to

9

check wether the distribution of the geometric phase was a normal distribution as theoretically expected.

The same process has then been applied repetitively for increasing drive amplitudes, in order to verify the consistence with the theoretical prediction on the visibility as a function of the drive field intensity. In fact the solid angle subtended to the path is closely related to the drive field intensity via

$$A = 2\pi \left(1 - \cos \left(\arctan \left(\frac{\sqrt{\Omega_x^2 + \Omega_y^2}}{\Delta} \right) \right) \right),$$

where A is the sought for solid angle and $\sqrt{\Omega_x^2 + \Omega_y^2}$ is the drive amplitude.

3.2 Application of noise to the 2-level system

Here, simulations have been written in order to reproduce the results of Ref. [6] and to predict the response of a 2-level system to external fluctuating fields.

Different sample sizes and different drive amplitude ranges have been used for the simulations. It is fundamental to use samples of sufficient size in order get statistically relevant results.

3.2.1 Noise symmetry

Besides its power distribution, the application of noise undergoes some further restrictions:

- *Symmetry in the geometric sequence*

  During the application of the geometric sequence, the same noise detuning has to be applied for both forward and reverse direction for the spin-echo experiment. In fact, by adding different noises to the detuning pulses before and after the spin-echo *pi*-pulse, the Hamiltonian would not follow exactly the same path backwards as he did onwards, and we would therefore get two different geometric phases for the two paths, whose sum is no more linked to the geometric phase we are interested in.

- *Symmetry among the samples*

  Creating a fixed list of noise values, which is reused for every amplitude at the beginning of the experiment leads to more regular results.

This could be avoided by considering much larger samples, but this would dramatically increase the computational cost of the process and therefore the time needed to perform it.

The resulting geometric phase acquired by the system in the presence of normally distributed constant detunings is shown in the histograms in Fig. 3.
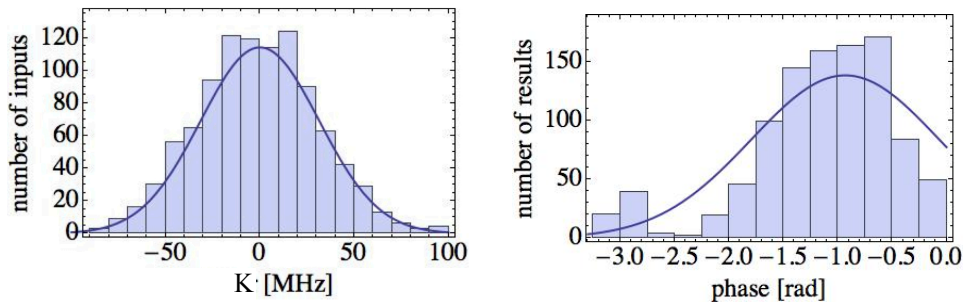

Figure 3: Distribution of applied noise detuning values and resulting phase for repeated geometric sequence experiment with noise power of $2 \cdot 5\pi$ MHz (equivalent to an FMDev value of 16 MHz) restricted to the first two levels. Expected curve also plotted. Despite a good agreement between the expected and actual curve of applied values of noise, the resulting phases are normally distributed around the expected value, but the variance does not agree with the theoretical one. The dimension of the sample is of 1000 elements.

The resulting phases and visibilities for sweeping amplitudes are also shown in Fig. 4 for different noise variances.

An important remark is that according to Ref.[7], because of the particular type of measurement (spin-echo) σ_α has to be scaled by a factor of 4.

3.3 Application of noise to the 3-level system

For the control parameters used in the experimental setup, approximating the transmon by a 2-level system is not justified. This is due to the increased ratio of Josephson energy to charging energy of the transmon, which brings the frequency of the first transition (from ground to first excited state) near to the one of the second transition (first to second excited state). Thus, our system is occasionally excited to the second excited state and , even though
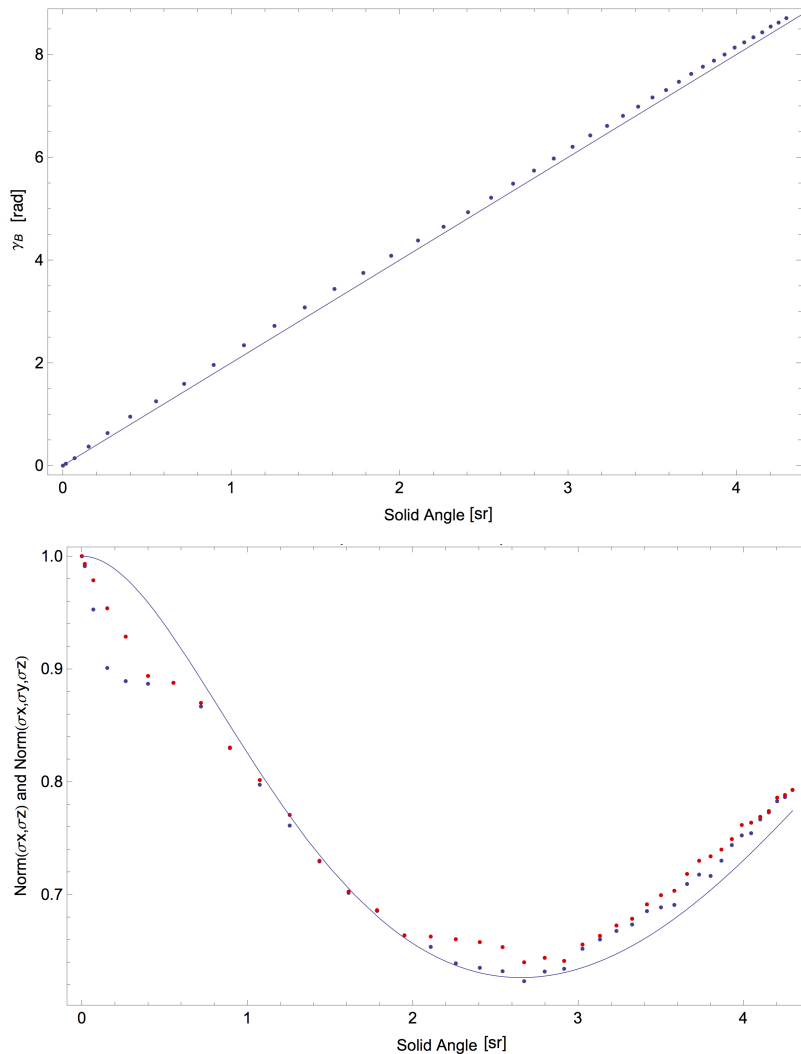
Figure 4: Geometric phase and visibility resulting form the average of repeated numerical solution of the Schrödingier equation restricted to the first two levels with $\Delta_0 = -2\pi\ 50$ and normally distributed noise values as a function of the solid angle described by the path of the Hamiltonian. For the visibilities, the length of the averaged Bloch vector (red) and its projection on the x-y plane (blue) have been plotted. A good agreement is displayed with theoretically expected curves [5, 6] (shown by continuous lines).

12

our computational subspace is spanned by the lowest two energy levels, we have to take the third energy level of the artificial atom into consideration. Therefore we extend our simulation to a 3 level system. In practice, we only had to increase the number of levels of the quantum system from 2 to 3, adapting the definitions of the Pauli matrices $\sigma_x, \sigma_y, \sigma_z$ to a 3-dimensional space.

Some of the results of the simulation are plotted in Fig. 5.

The resulting phases and visibilities as a function of solid angle are also shown for different noise variances. Compared to the 2-level simulations, the results for the 3-level system are less precise for large solid angles and have a much greater computational cost.

3.4   Simulation of noise

Some attempts to simulate non-constant noise have been made, in order to be closer to the experiment.

3.4.1   Lorentzian noise

In order to create noise described by an OU process, we begin by distributing some random Lorentzian distributed points in the frequency space with expected value f_3 and bandwidth Γ_3, each of these points representing the frequency of a mode of the future noise function. As a second step, we have assigned to each of those points a real normal $(0, \sigma_3)$ distributed random number, where 0 is the expected value of the normal distribution and σ_3 is its standard deviation. The assigned number represents in our simulation the amplitude of the mode whose frequency was chosen in the previous step. We now want to assign a random phase to the mode, and this has been done by multiplying the amplitude value by a complex random number uniformly distributed on the unit circle. As a last step, an inverse Fourier transform has been applied to the generated points, and the resulting function is the wanted noise function. Such a function and its power distribution are displayed in Fig. 6.

3.4.2   White noise

We aim in this section to create a function displaying the features of bandwidth-limited Gaussian white noise, i.e. a constant but low-pass filtered spectral
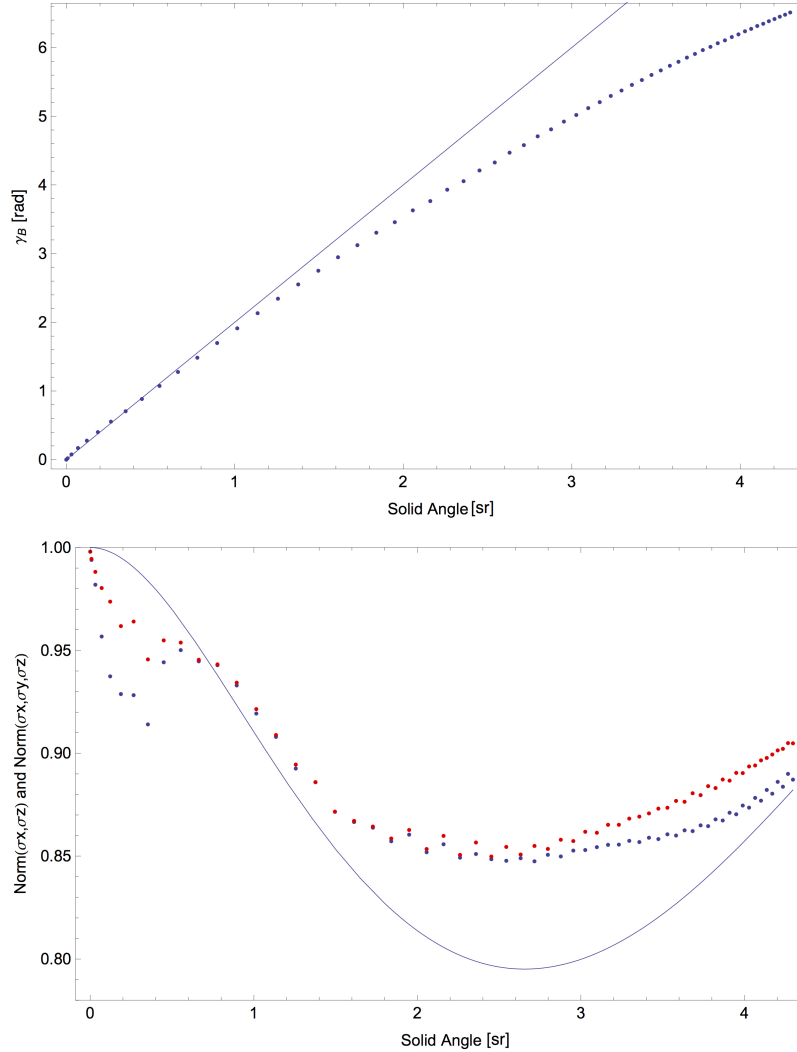
Figure 5: Geometric phase and visibility resulting form the average of repeated numerical solution of the Schrödingier equation extended to the third level with $\Delta_0 = -2\pi\,50$ and normally distributed noise values as a function of the solid angle. For the visibility, the length of the averaged Bloch vector (red) and its projection on the x-y plane (blue) have been plotted. A good agreement is displayed with theoretically expected curves [5, 6] (shown by continuous lines). For a more precise prediction of the geometric phase, the theory has to be extended to the third level of the system as in Ref. [8].
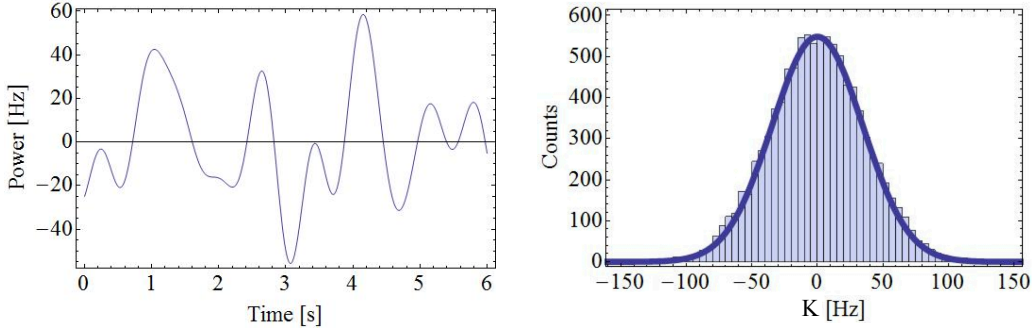
Figure 6: Noise Function with Lorentzian spectrum. The power distribution of the created function is also shown with the expected one (blue continuous line: normal $(0, \sigma_3)$ distribution).

density and a Gaussian power distribution (the distribution of the values assumed by the noise function should be normal with expected value 0 and standard deviation σ_3). To this end we divide the time interval of our interest (the one for which we want to create a noise function) into constant steps, whose length is half of the minimum period of the noise oscillation (maximum frequency component of the noise). To each of those points, a normal $(0, \sigma_3)$ number is assigned. These random numbers are intended to be the "peaks" of our noise function, which is the given by a spline interpolating function connecting all of them. A resulting function and its power distribution are displayed in Fig. 7.

3.5   Discussion of the simulation results

The simulations restricted to the lowest two levels have shown a very good agreement with the theoretically expected values in the case of very low frequency noise (constant during every sample). In particular, the phase of the qubit as a function of solid angle fits very well to Berry's theory. There are some discrepancies between theoretical and simulated visibilities. These are probably due to the non-vanishing adiabaticity of the simulation.

Including the third level of the qubit in our simulations, we see that the role of statistics becomes more relevant: the resulting phases and visibilities are more widely distributed and we have to average more. The phase of the qubit as a function of solid angle agrees with the theoretical values up to
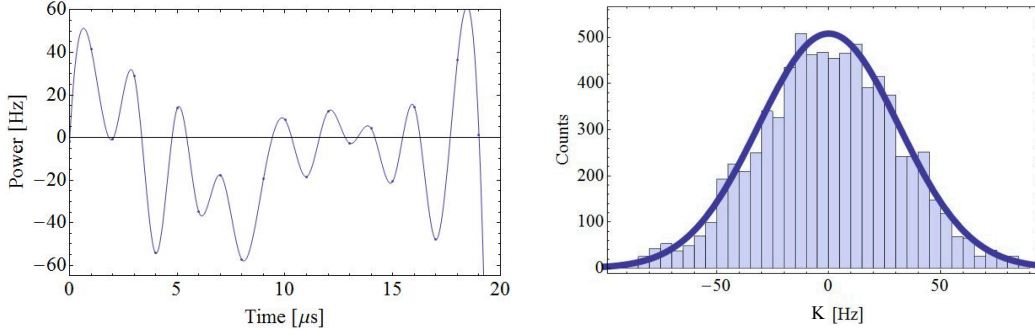
Figure 7: Noise Function with white bandwidth-limited spectrum. The power distribution of the created function is also shown with the expected one (blue continuous line: normal $(0, \sigma_3)$ distribution).

threshold value (around $A \approx 1.5$ sr in Fig. 5), as well as the visibility of the qubit. We then notice deviations from the expected values. They are due to the presence of the higher levels.

A comparison between simulations and expected values therefore shows that even slight variations from the theoretical assumptions, e.g. adiabaticity or noise distributions, lead to discrepancies between theory and simulations. Moreover, we see that for small noise powers, many samples are needed in order to perform relevant comparison between theory and simulations.

4   Experimental measurements

In order to verify experimentally the theoretical expectations and the simulation results, we carry out measurements of the geometric phase of a transmon exposed to noise.

A simplified circuit diagram of the experimental setup is displayed in Fig. 8 below. For detailed explanation we refer to Refs.[8, 9].
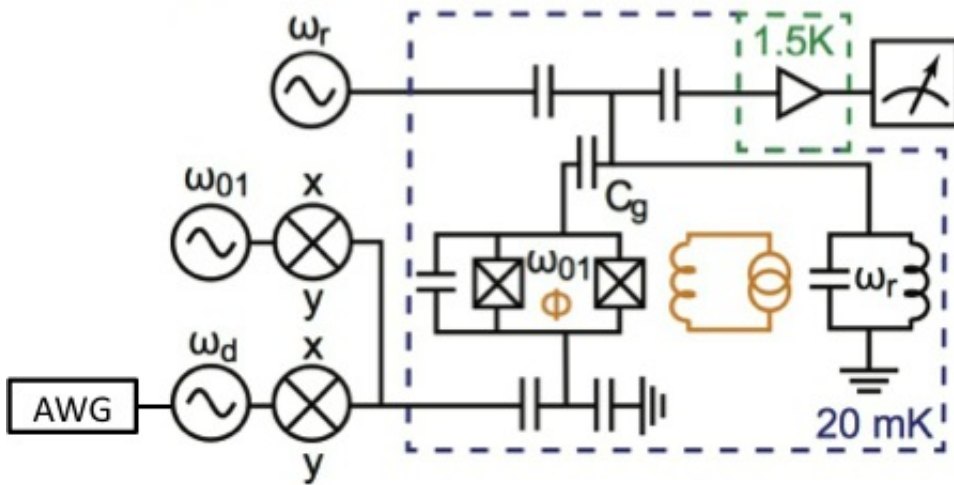

Figure 8: Scheme of the measurement circuit [8]. Noise is applied only in z-direction which in our system corresponds to a detuning fluctuating around an average value Δ_0. Concretely, this has been done by connecting a low-pass filtered arbitrary wave generator (AWG) that outputs white gaussian noise to the frequency modulation port of the signal generator used to produce the off-resonant pulses.

4.1   Qubit calibrations

In a first part of the experiment, we calibrated the experimental setup in order to measure the geometric phase and to observe its response to noise. The calibration procedure can be summarized as follows:

- *Resonance frequency*

The transition frequency ω_{01} between the ground and first excited state of the qubit has to be found. The DC offsets for the IQ-mixer sending the resonant pulses have to be calibrated. Here, $\omega_{01} = 5.112$ GHz.

- *Calibration of π-pulses*

  The amplitude of the resonant π pulses has to be calibrated on x and y quadratures.

- *Amplification*

  After mixing, the microwave pulses are amplified before being sent to the qubit. Calibration of the amplifier has to be performed.

4.1.1 Calibration check

To verify the calibration, we measured the resonator response after preparing the qubit in the excited state $|1\rangle$ and fitted the results to the cavity-Bloch equations. The results of those measurements for two different numbers of averages are shown in Fig. 9.

4.2 Experimental parameters

The parameters of the geometric sequence used to perform our measurements are listed in Tab. 1.

Parameter	Experimental parameters	Simulation parameters
Drive range Ω	$\{0, 3, ..., 90\}$ MHz	$\{0, 5, ..., 150\}$ MHz
Detuning Δ_0	-35 MHz	$\{-35, -50\}$ MHz
Resonance freq. ω_{01}	5.112 GHz	30 MHz
π pulse length	20 ns	10 ns
Averages	$\sim 2 \times 10^6$	10^3
Noise power	$\{0, 1, ..., 16\}$ MHz	$\{0, 8, 16, 32\}$ MHz

Table 1: Characteristic values of the listed parameters for both simulation and experiment.

As mentioned in section 3.1 we directly measure the geometric phase because the dynamic phase of the qubit is cancelled out with the spin-echo method. The complete state of the qubit was determined with state tomography.

4.3   Noise apparatus

Experimentally, the application of noise to the z-component of the Hamiltonian of our system, is achieved by adding noise to the average detuning Δ_0. To implement this in the experiment, the low-pass filtered output of an AWG has been connected to the modulation port of the signal generator for the off-resonant pulses. Three different filters have been used in our experiment, with cutoff frequencies of 400 kHz, 500 kHz and 1 MHz. Keeping the AWG output power fixed, at the modulation port of the signal generator the amplitude of the noise pulses was scaled (the pulses were amplified) in order to set the power of the noise sent to the qubit. In this way we produced gaussian white noise at fixed power with the AWG, whose maximum frequency was set by the low-pass filter and whose power was scaled before being added to the average detuning Δ_0.

The measurements are then carried out by measuring the geometric phase as a function of the solid angle first, and remeasuring it while applying a range of noises sweeping the FM modulated deviation of the signal generator.

4.4   Data analysis and results

The measurements of the experiment, voltage time traces, are stored and analyzed to extract the qubit populations. Another Mathematica program then compares the results from different noise amplitudes, plotting the visibility as a function of solid angle for every noise amplitude and comparing it to theory. A fitting of the experimental results with the theoretical curves have been performed to deduce from the best fitting curve the values of applied noise power according to Eq.8 without dynamic term. Because of the bad fits, this process has actually been applied only to values of visibilities corresponding to drive amplitudes below a certain threshold (usually $\Omega_{threshold}/2\pi \approx 40$ MHz). It is worth noticing that the visibility at zero drive amplitude is 1 for the simulated system, whereas experimental measurements display visibilities around 0.8. This is due to the finite lifetime of the qubit, which is assumed to be infinite in the simulations. We normalize the visibility dividing visibility results for different noises by the visibility measured for the same probe without noise. So the visibility at zero drive is 1.

During the analysis process, we have found out that averaging over 2×10^6 sample yielded to imprecise results. The number of averages per qubit population measurement has then been doubled to 4×10^6.
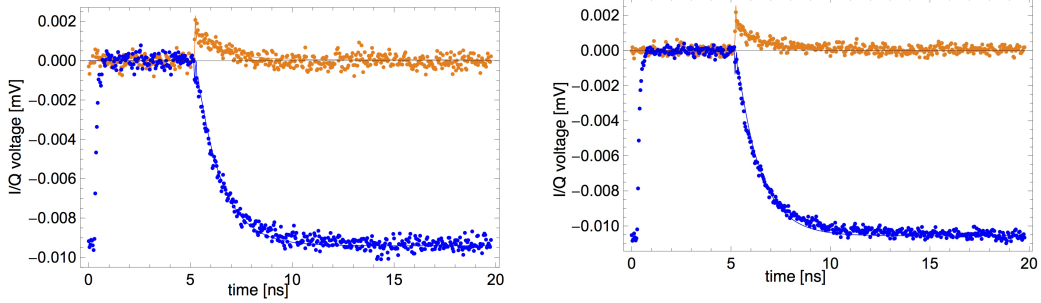
Figure 9: Population measurements for different numbers of averages done by measuring the output voltages of the I and Q quadratures (blue and orange points respectively) at the end of the resonator. It can be noticed they the spread of the measurements is much bigger in the first plot (2×10^6 averages) than in the second (4×10^6 averages). The fitting of the measurements to the cavity-Bloch equations is also shown (continuous lines).
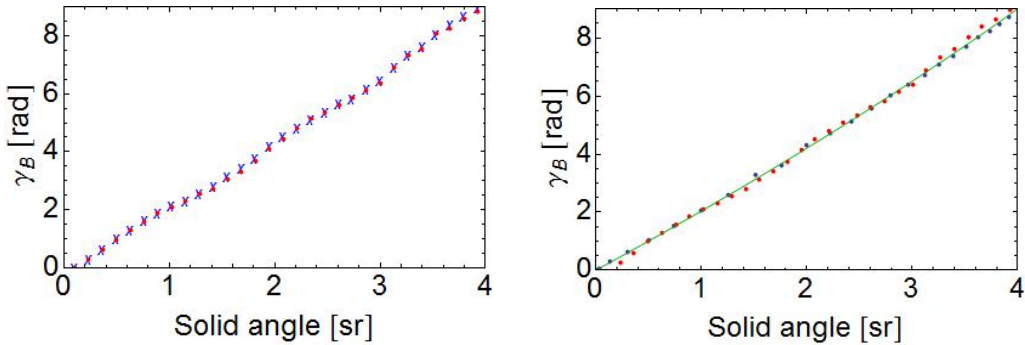

Figure 10: Experimental geometric phase measurements as a function of solid angle are shown in the plot on the left both in the presence (blue crosses) and in the absence (red points) of noise (FMDev = 16 MHz). No noticeable difference can be seen in the two cases. In the figure on the right a comparison of the average geometric phase in the presence of noise (FMDev = 16 MHz) for theory extended to the third level (green continuous line), simulations (blue points) and experiment (red points). We see a good agreement in all three cases.

In Figs. 11, 12 and 13, experimental visibility measurements and fitting curves ignoring points corresponding to drive amplitudes larger than a

20

threshold value $\Omega_{threshold}$ (indicated by a red line in the plots) are displayed for the different low-pass filter implemented (respectively 400 kHz, 500 kHz and 1MHz). The fitting curves are $\exp(-\sigma_\alpha^2/2)$, where σ_α is given by Eq. 8 and the fitted parameters are σ_3 and Γ_3.
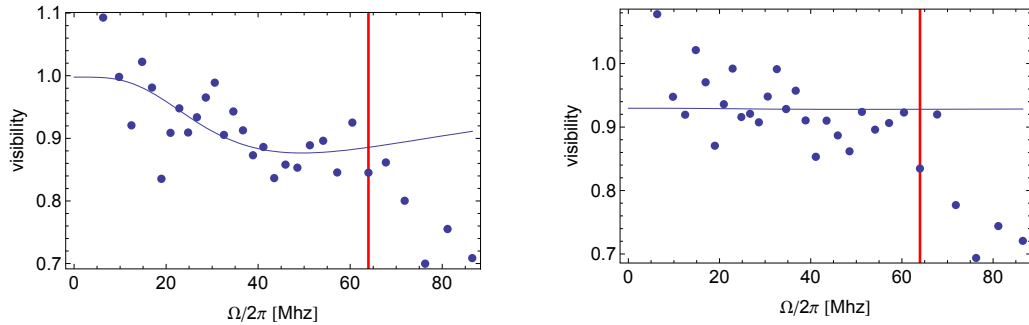
/

Figure 11: Visibility measurements for noise with 400kHz filter (2×10^6 averages) for different drive noise intensities (FMDev is respectively 16 MHz and 8 MHz). A fitting curve is plotted in the first image, whereas in the second the points are so scattered with respect to the oscillation of the function that no fit has been found. From the fitting curve, the applied noise power can be deduced and compared with the actually applied one as in Fig. 14.
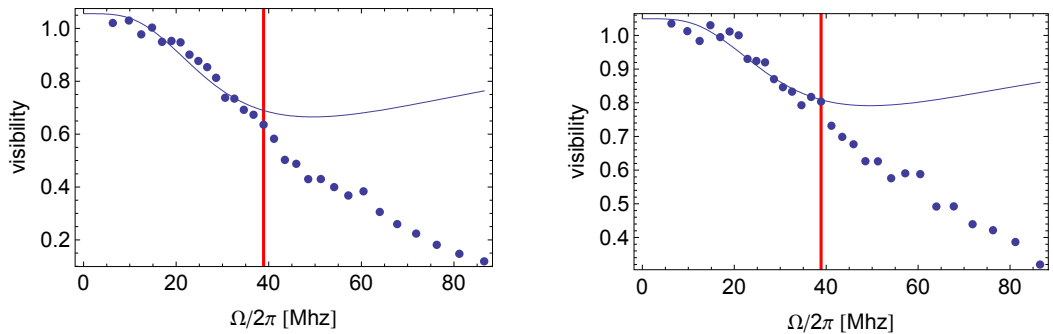
/

Figure 12: Visibility measurements for noise with 500 kHz filter (4×10^6 averages) for different drive noise intensities (FMDev is respectively 16 MHz and 12 MHz). Fitting curves are plotted as well.
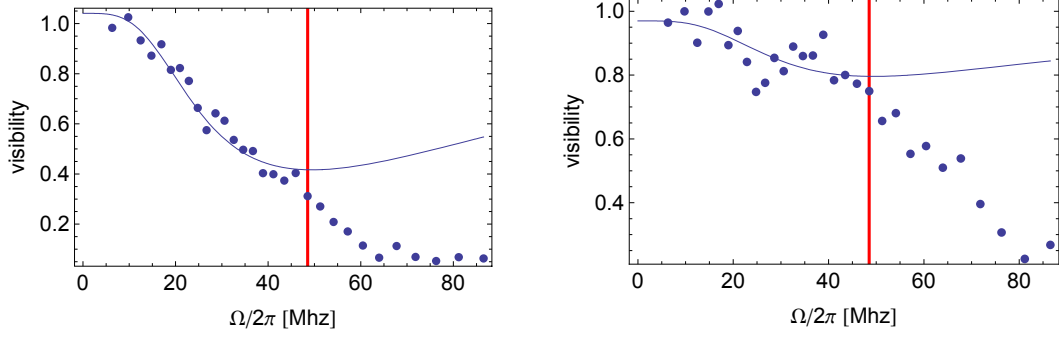
21

/

Figure 13: Visibility measurements for noise with 1 MHz filter (4×10^6 averages) for different drive noise intensities (FMDev is respectively 16 MHz and 12 MHz). Fitting curves are plotted as well.
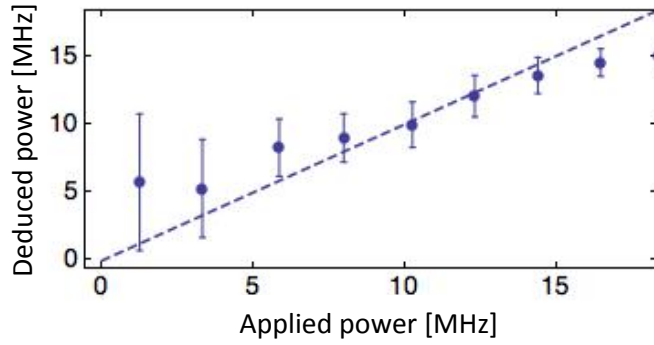

Figure 14: Comparison between the actually applied noise power and the one, which was deduced from the theoretical curves fitting the experimental results of the visibility varying σ_3 and Γ_3. Errors of the deductions are also shown. We can notice a good agreement of the actual and deduced noise power in the interval $\sigma_{exp} \in [8, 15]$ MHz.

4.5   Discussion of the experimental results

As in the simulations, we confirmed experimentally the importance of averaging over more samples in order to balance the effects of the intrinsic noise affecting our experiment (hindering us from single-shot measurements) and to reduce the scatter in the measured visibilities. The agreement with theory of the experimental results is good only in some ranges of noise power and drive amplitude:

- For small noise powers (FMDev ≤ 6 MHz) the decrease in visibility is small and the scatter in the measured visibilities is too large to make fits.

- For too big amplitudes a sensible discrepancy with theoretical expectations can be seen in every experimental plot. In fact, it can be seen that a fit of only the measurements corresponding to drive amplitude smaller than a given value display a good agreement up to the fitting threshold and a strong disagreement above it. Fittings to all experimental values did not work and have therefore not been displayed. Reasons for this disagreement could be the non-Lorenzian form of experimental noise, as well as the possible role played by the strength of the drive amplitude Ω.

On the other hand, the average of the experimentally measured geometric phases as a function of drive amplitude agrees well with the averaged geometric phase resulting from simulations extended to three levels.

Comparison between the deduced noise powers and the actually applied ones (Fig. [?]) show that the fitting of a limited sample of experimental points leads to realistic deductions only for an interval of noise powers.

5 Conclusions and outlook

In this thesis the resilience to white gaussian noise of a Berry phase measured on a transmon has been both simulated and experimentally tested. As expected, the Berry phase is not sensibly affected by the presence of an external fluctuating field.

Furthermore, measurements of the geometric phase and visibility of the system have been compared to the theoretical predictions for a two levels quantum system. Those predictions have been found to be appropriate for experimental parameters in the intervals FMDev $\in [8, 15]$ MHz (corresponding approximately to $\sigma_{exp} \in [2.6 \cdot 2\pi, 4.8 \cdot 2\pi]$) and $\Omega/2\pi \lesssim 50$ MHz. Outside those intervals of noise power and drive amplitude, discrepancies between theory and experiment appear.

In the future, the models of noise studied in this project could be developed to describe the experimental noise more accurately, leading to an understanding of the causes of the discrepancies between theory and experiment and possibly to a theory ruled by more realistic assumptions.

References

[1] M. Nielsen, I. Chuang, *Quantum Computation and Quantum Information*, (Cambridge University Press, Cambridge, 2000)

[2] A. Blais *et al.*, Physical Review A **69**, 062320 (2004)

[3] J. Chirac and P. Zoller, *Physical Review Letters*, **74** 024091 (1995)

[4] D. Loss and D. P. DiVincenzo, *Physical Review A* **75**, 120 (1998)

[5] M.Berry, *Proc. R. Soc. Lond.* A, **392**, 45 (1984)

[6] G. De Chiara and G. Palma, *Physical Review Letters* **91**, 090404 (2003)

[7] S. Filipp *et al.*, *Physical Review Letters* **102**, 030404 (2009)

[8] S. Berger *et al.*, *arXiv:***1204**.1278v1 (2012)

[9] P. Leek *et al.*, *Science* **318**, 1889 (2007)

[10] A. Blais *et al.*, *Physical Review A* **75**, 032329 (2007)

Acknowledgements